8-1-2017

Regional Sensitivities of Seasonal Snowpack to Elevation, Aspect, and Vegetation Cover in Western North America

Nancy F. Glenn
Boise State University

AGU PUBLICATIONS

Water Resources Research

RESEARCH ARTICLE
10.1002/2016WR019374

Key Points:
- At watershed-scales elevation explained the most variability in forest and shrub snow depths but aspect was more important in alpine areas
- The variability in snow depth explained by aspect and vegetation varied with incoming shortwave to incoming net radiation and wind speed
- Variability in physiographic effects on snow depth driven by energy differences suggests differential sensitivities to expected climate changes

Correspondence to:
C. J. Tennant,
chris.tennant@berkeley.edu

Citation:
Tennant, C. J., A. A. Harpold, K. A. Lohse, S. E. Godsey, B. T. Crosby, L. G. Larsen, P. D. Brooks, R. W. Van Kirk, and N. F. Glenn (2017), Regional sensitivities of seasonal snowpack to elevation, aspect, and vegetation cover in western North America, *Water Resour. Res.*, *53*, 6908–6926, doi:10.1002/2016WR019374.

Received 16 JUN 2016
Accepted 12 JUL 2017
Accepted article online 15 JUL 2017
Published online 17 AUG 2017

Regional sensitivities of seasonal snowpack to elevation, aspect, and vegetation cover in western North America

Christopher J. Tennant[1], Adrian A. Harpold[2], Kathleen Ann Lohse[3], Sarah E. Godsey[3], Benjamin T. Crosby[3], Laurel G. Larsen[1], Paul D. Brooks[4], Robert W. Van Kirk[5,6], and Nancy F. Glenn[7]

[1]Department of Geography, University of California at Berkeley, Berkeley, California, USA, [2]Department of Natural Resources and Environmental Science, University of Nevada, Reno, Nevada, USA, [3]Department of Geosciences, Idaho State University, Pocatello, Idaho, USA, [4]Department of Geology and Geophysics, University of Utah, Salt Lake City, Utah, USA, [5]Henry's Fork Foundation, Ashton, Idaho, USA, [6]Department of Mathematics, Humboldt State University, Arcata, California, USA, [7]Department of Geosciences, Boise State University, Boise, Idaho, USA

Abstract In mountains with seasonal snow cover, the effects of climate change on snowpack will be constrained by landscape-vegetation interactions with the atmosphere. Airborne lidar surveys used to estimate snow depth, topography, and vegetation were coupled with reanalysis climate products to quantify these interactions and to highlight potential snowpack sensitivities to climate and vegetation change across the western U.S. at Rocky Mountain (RM), Northern Basin and Range (NBR), and Sierra Nevada (SNV) sites. In forest and shrub areas, elevation captured the greatest amount of variability in snow depth (16–79%) but aspect explained more variability (11–40%) in alpine areas. Aspect was most important at RM sites where incoming shortwave to incoming net radiation (SW:NetR↓) was highest (∼0.5), capturing 17–37% of snow depth variability in forests and 32–37% in shrub areas. Forest vegetation height exhibited negative relationships with snow depth and explained 3–6% of its variability at sites with greater longwave inputs (NBR and SNV). Variability in the importance of physiography suggests differential sensitivities of snowpack to climate and vegetation change. The high SW:NetR↓ and importance of aspect suggests RM sites may be more responsive to decreases in SW:NetR↓ driven by warming or increases in humidity or cloud cover. Reduced canopy-cover could increase snow depths at SNV sites, and NBR and SNV sites are currently more sensitive to shifts from snow to rain. The consistent importance of aspect and elevation indicates that changes in SW:NetR↓ and the elevation of the rain/snow transition zone could have widespread and varied effects on western U.S. snowpacks.

1. Introduction

Understanding the processes controlling snowpack-topography relationships in mountain landscapes is critical for quantifying the sensitivity of ecosystems [*Elsen and Tingley*, 2015] and water resources to changes in climate and vegetation [*Goulden and Bales*, 2014]. Streamflow amount [*Berghuijs et al*., 2014], timing [*Stewart et al*., 2005; *Ryberg et al*., 2015], and summer low flows [*Godsey et al*., 2013] all exhibit strong correlation with snow water equivalent and/or the fraction of precipitation falling as snow. Forest greenness [*Trujillo et al*., 2012] and the amount and timing of carbon sequestration and efflux [*Brooks et al*., 2011; *Monson et al*., 2002; *Stielstra et al*., 2015] are also strongly regulated by snowpack amount. Given the high certainty of future warming [*Pepin et al*., 2015], potential shifts in precipitation amount [*Seager et al*., 2013] and changes in the extent, density, and activity of vegetation [*Goulden and Bales*, 2014], mountain snowpack will likely undergo changes. An important step in improving predictions of the future effects of climate change on snowpack and snow-vegetation interactions is quantifying seasonal snowpack patterns across elevation gradients in mountain regions that vary in their climatic and vegetation characteristics.

Seasonal snowpack is affected by complex interactions between climate, topography, and vegetation. Differences in precipitation amount and energy available for ablation (melt and sublimation) change with elevation and season [*Anderson et al*., 2014; *Clark et al*., 2011; *Roe*, 2005]. Variability in slope and aspect affects the radiation budget and wind loading and leads to heterogeneous patterns of snow cover [*Elder et al*., 1991; *Winstral et al*., 2013]. Vegetation intercepts snowfall, shades snowpack [*Musselman et al*., 2008; *Veatch*

et al., 2009], alters snowpack albedo [*Pomeroy and Dion*, 1996], affects shortwave radiation scattering and partitioning of shortwave and longwave radiation [*Rinehart et al*., 2008; *Broxton et al*., 2015], and intercepts wind-blown snow [*Hiemstra et al*., 2002]. Currently, many of the fine-scale processes that are modified by vegetation are difficult to accurately parameterize in snowpack energy budget models, with potentially important consequences for larger-scale water and energy budgets [*Broxton et al*., 2015], particularly in forested terrain [*Essery et al*., 2009; *Rutter et al*., 2009]. Because of spatial variability in mass and energy inputs and relatively sparse climate and snowpack observations, we still lack a complete understanding of how topography and vegetation affect snowpack dynamics, how these effects differ by elevation, and the varying sensitivities of this system to projected changes in climate and vegetation.

The increasing availability of snow depth products from airborne light detection and ranging (lidar) surveys [e.g., *Cline et al*., 2009; *Grünewald et al*., 2014; *Harpold et al*., 2014a; *Hedrick et al*., 2015; *Kirchner et al*. 2014; *Painter et al*., 2016; *Zheng et al*., 2016] is particularly exciting because they offer a high-resolution, spatially extensive view of how regional-scale climate characteristics interact with local topography and vegetation to produce patterns of seasonal snow accumulation. For example, *Kirchner et al*. [2014] used airborne lidar surveys of snow depth and topography in the Southern Sierra Nevada Mountains, CA, USA, to document rates of snow depth increase with elevation that were not revealed by local meteorological stations. Also in the Southern Sierra, *Zheng et al*. [2016] demonstrated the importance of pixel resolution when estimating snow accumulation in forested and open terrain. *Grünewald et al*. [2014] used airborne lidar and photogrammetry surveys from the Swiss Alps and Spanish Pyrenees to demonstrate consistent declines in snow depth at high elevations that contrasted the spatial trend of increasing snow depth found at lower and mid elevations. They attributed these declines to land cover being dominated by steep, rocky exposures [*Grünewald et al*., 2014]. *Kirchner et al*. [2014] also found declines in snow depth at high elevations that contrasted increases in lower-elevations and midelevations but suggested that these declines were caused by depletion of orographic precipitation.

Here we build on a long tradition of linking snow distribution to physiography and climate [e.g., *Adams*, 1976; *Balk and Elder*, 2000; *Elder et al*., 1991; *Steppuhn and Dyck*, 1974], but leverage the increased availability of airborne lidar-derived products to evaluate these interactions at higher resolutions and across greater elevation ranges than before. Regional-scale airborne lidar surveys (18–294 km^2) of snow depth, topography, and vegetation from five sites distributed between the Rocky Mountains, Northern Basin and Range, and Sierra Nevada mountains of the western U.S. were used to test four hypotheses that are based on a rich history of snow distribution studies. (H1) Elevation will be an important predictor of snow depth variability across all sites. (H2) Mean snow depths on different aspects and different vegetation classes (i.e., alpine, forest, and shrub areas) will exhibit significant differences because of variability in ablation. (H3) Slope and aspect will capture more snow depth variability at sites with greater shortwave inputs (high SW:NetR↓, defined in section 3.3) and high wind speeds. (H4) We also expect shading by tall vegetation to be more important in places that receive greater shortwave radiation (high SW:NetR↓).

Building on our evaluation of these hypotheses, we propose potential sensitivities of snowpack to shifts in SW:NetR↓ and vegetation and discuss how the impacts of these changes could vary between sites. We also propose a simple temperature-based metric to estimate watershed-scale sensitivity of snowpack to warming and shifts from snow to rain.

2. Data

2.1. Elevation, Snow Depth, and Vegetation Height

Recent studies have validated the use of airborne lidar for measuring snow depth in open and forested terrain with vertical accuracies typically in the decimeter range [*Deems et al*., 2013; *Harpold et al*., 2014a; *Hopkinson et al*., 2004; *Kirchner et al*., 2014; *Tinkham et al*., 2014]. The snow depth, bare earth, and canopy height models used in this study were published and verified using field-based surveys reported in *Harpold et al*. [2014a] and *Tinkham et al*. [2014] and are from U.S. National Science Foundation Critical Zone Observatories (CZOs) in mountainous regions of the western U.S. (Figure 1): Boulder Creek Watershed (BCW) and Jemez River Basin (JRB) in the Rocky Mountains, the Reynolds Creek Experimental Watershed (RCEW) in the Northern Basin and Range, and the Kings River Experimental Watershed (KREW) and Wolverton Basin (WOLV) in the Sierra Nevada mountains.

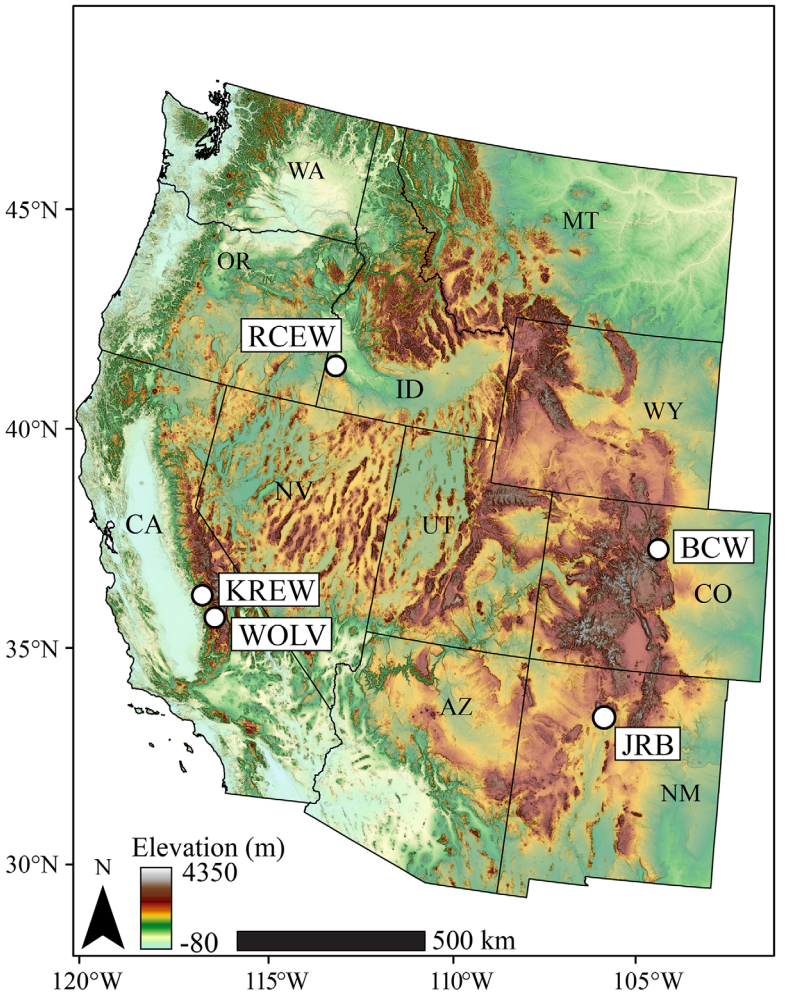

Figure 1. Map of western U.S. showing elevation, topography, and the locations of the snow-on-off airborne lidar surveys: Boulder Creek Watershed (BCW) and Jemez River Basin (JRB) in the Rocky Mountains, Reynolds Creek Experimental Watershed (RCEW) in the Northern Basin and Range, and Kings River Experimental Watershed (KREW) and Wolverton Basin (WOLV) in the Sierra Nevada. The study sites are part of the Boulder Creek, Jemez River Basin-Santa Catalina, Reynolds Creek, and Sierra Nevada Critical Zone Observatories, respectively.

All snow-depth surveys were taken at or near peak accumulation [*Harpold et al.*, 2014a; *Tinkham et al.*, 2014]. However, given the high relief of the sites and the different flight dates, melt likely occurred at lower elevations but not at higher elevations and the magnitude of these effects probably varied between the sites. It is also important to note that our study focuses on the characterization of snow depth and not snow water equivalent. Detailed observations capturing the spatial variability in snow density from the day of the snow-covered flights were not available. Because snow depth varies over a much greater range than snow density [*Sturm et al.*, 2010] we do not expect that converting depth to water equivalent would result in significant changes to the interpretations presented here. Because forest-cover at the sites was composed of relatively homogenous vegetation types (catalogued in section 4) we used vegetation height as a proxy for interception and solar shading, instead of computing additional canopy metrics. The effects of differences in tree species on snow interception and shading were likely most pronounced at RCEW where forest stands were either homogenous aspen or Douglas fir [*Tinkham et al.*, 2014]; the other sites are dominated by mixed conifer forests [*Harpold et al.*, 2014a; also see sections 4.2–4.5].

The National Center for Airborne Laser Mapping (NCALM), along with the cooperation of the CZOs, conducted the snow-covered surveys for all of the sites in 2010, except for RCEW, which was surveyed by Watershed Sciences, Inc. in 2009. The accuracy of the LiDAR-derived snow depths at BCW, JRB, KREW, and WOLV were evaluated using ultrasonic snow depth sensors installed perpendicular to the snow surface in both forested and open terrain [*Harpold et al.*, 2014a] and at RCEW, lidar snow depth accuracies were

quantified via manual snow survey measurements [*Tinkham et al*., 2014]. The lidar snow depth root mean squared errors are reported in the site descriptions (sections 4.2–4.5).

The 1 m resolution gridded products of snow depth and bare-earth elevations produced by NCALM and the Boise Center Aerospace Laboratory (BCAL) [*Shrestha*, 2016] were aggregated to 3 m resolution to reduce the bias of DEM derivative products (e.g., slope and curvature; *Kienzle* [2004]). All snow depths on slopes greater than 50° (<2% of snow-covered area at all sites) were removed because of vertical bias of lidar on steep slope angles [*Deems et al*., 2013]. All open water bodies, buildings, roads or any other erroneous data points produced during gridding and interpolation of snow depth (e.g., edge effects) were identified by hand, masked, and removed to reduce the error of our analyses. All lidar mapped areas that met the criteria above, including those that were snow-free, were used for analysis. For further details on the lidar snow depth accuracies and methods used to generate the gridded products, see *Harpold et al*. [2014a], *Kirchner et al*. [2014], and *Tinkham et al*. [2014].

2.2. Climate Data

Gridded outputs of hourly air temperature (at 2 m above surface), potential evapotranspiration, total precipitation, surface incident longwave radiation, surface incident shortwave radiation, and wind speed (at 10 m above surface) from the National Land Data Assimilation System 2 (NLDAS) were used to characterize the meteorological conditions of the sites from 1 November until the respective flight date for each CZO. NLDAS uses four land surface models (NOAH, SAC-SMA, VIC, and Mosaic) to generate 1/8° (32 km resolution) gridded estimates of the water and energy balance for the conterminous U.S. and other portions of North America at an hourly time step [*Xia et al*., 2012]. NLDAS outputs were accessed using NASA's GIOVANNI data portal (http://giovanni.sci.gsfc.nasa.gov/giovanni/). We used these coarser-resolution products because they provided a consistent methodology and covered a larger spatial extent than could be accurately inferred from using the sites' instrumented stations alone. At all sites, the "footprints" of the LiDAR and NLDAS grids matched closely except at KREW where the lateral extents of the NLDAS cells extend slightly (~3 km on average) beyond that of the lidar snow-covered extent.

3. Methods

To evaluate our hypotheses (H1–H4), we used a combination of multivariate regression, ANOVA, and correlation statistics. In the following sections, we describe the details of the data analyses, statistical tests, and the computation of a proposed metric to estimate watershed-scale snow sensitivity to shifts from snow to rain.

3.1. Snow Depth and Elevation

To determine regional changes in snow depth with elevation, we binned the snow depth values by elevation and reported the mean snow depth for each elevation bin. The Freedman and Diaconis rule [*Freedman and Diaconis*, 1981] was used to provide an unbiased method for selecting bin sizes. To compute the first derivative of snow depth and elevation (dS/dE) in a consistent manner across the sites, we fit a shape preserving interpolant to the relationship between mean snow depth and elevation and computed the derivative at 10 m elevation spacing using a fourth-order central difference.

3.1.1. Snow Depth Residuals

Factors associated with elevation (e.g., air temperature and orographic precipitation effects) tend to influence snow patterns over larger spatial scales than factors associated with aspect, slope, and vegetation (e.g., drifting and differential ablation). For example, *Clark et al*. [2011] reported that the dominant processes that generate snow depth variability at hillslope scales (1–1000 m) are preferential deposition of windblown snow, sloughing and avalanching, and interception and sublimation from forest canopy. At watershed scales (100–10,000 m), *Clark et al*. [2011] found that hillslope scale variability averaged out and snow depth formed a strong relationship with elevation. These results generally agree with those presented in *McKay and Gray* [1981] and *Tarboton et al*. [2001] who also discussed the importance of orographic precipitation effects for setting large-scale snow patterns. Because all of the lidar flights covered a large area (18–294 km^2) it was important to remove the effects of elevation on snow depth before testing for effects related to aspect and vegetation. We fit polynomial equations (up to order 13) to the mean snow depth-elevation relationships and used Akaike Information Criterion (AIC) to select the best fit. These snow depth trends with elevation were then differenced from the snow depth values to obtain snow depth residuals. To

ensure independence and avoid issues associated with spatial autocorrelation in the ANOVA and multivariate regressions (sections 3.2.2 and 3.2.3), we used random samples of snow depth residuals and physiographic predictors. The random samples were generated from a pseudorandom number generator and were drawn from a uniform distribution.

3.2. Effects of Aspect and Vegetation on Snow Depth

3.2.1. Aspect and Vegetation Cover

We computed a number of categorical and numerical variables for use in the ANOVA and regression analyses to assess the effects of aspect and vegetation on snow depth. The canopy height models generated by NCALM and BCAL from the snow-off flights were used to delineate three vegetation classes—alpine, forest, and shrub—that were used as hierarchical variables in the ANOVA and multivariate regressions. The alpine zone references areas above the tree line, where the tree line was defined as a threshold elevation above which vegetation heights were continuously <2 m. Forest and shrub were designated as areas below the tree line elevation where vegetation heights were >2 m and <2 m, respectively. The snow-off bare-earth elevation models were used to compute grids of slope and aspect using the Spatial Analyst toolbox in ArcMap 10.2 (Environmental Systems Research Institute, Redlands, CA) and were used in the ANOVA and multivariate regressions.

3.2.2. Effects of Vegetation Cover on Mean Snow Depth

To evaluate if groupings based on aspect and vegetation class resulted in statistically different snow depths, we performed analysis of variance (ANOVA) and Tukey-Kramer Honestly Significant Differences (HSD) post hoc tests to evaluate pairwise comparisons. For each site, the random samples of snow depth residuals were grouped into alpine, forest, and shrub ($n = 120$ for each vegetation class) and were subdivided into northeast (NE; 0–90°), southeast (SE; 90–180°), southwest (SW; 180–270°), and northwest (NW; 270–360°) aspects. We tested the main effects (aspect and vegetation class) and their interaction (aspect $\times$ vegetation class). Testing the interaction term was important because it revealed whether or not the effects of aspect depended on vegetation class or vice versa. Because the design was unbalanced, we tested both model orderings to confirm the main effects. The ANOVA and post hoc Tukey-Kramer HSD test were performed using base utilities in the *R* statistical computing environment [*R Core Team*, 2013].

3.2.3. Multivariate Regressions on Snow Depth

To evaluate the effects/relative importance of physiography on snow depth, we used multivariate regression [e.g., *Chang and Li*, 2000; *Grünewald et al*., 2013; *Jost et al*., 2007; *Lopez-Moreno and Nogues-Bravo*, 2006]. Again, we employed a simple hierarchical approach by dividing a random sample of a site's snow depth values into its respective vegetation classes (forest, shrub, and alpine, if present; $n = 120$ for each vegetation class). For each of these samples, we computed the coefficient of determination (R^2 value) between the polynomial-based snow depth trend with elevation (section 3.1) and the random sample of snow depth and attributed this coefficient as the variability in snow depth explained by elevation.

Snow depth residuals for each vegetation class were regressed against eastness (sine(aspect) $\times$ slope), northness (cosine(aspect) $\times$ slope), slope, and vegetation height (treated as continuous within a given vegetation class). These covariates were used as proxies for processes that influence patterns of snow depth (e.g., solar radiation, wind loading, preferential deposition, and interception). All two-way interaction terms for the variables above (e.g., eastness $\times$ vegetation height, northness $\times$ vegetation height, etc.) were included in the model structure to capture potential nonlinear effects and dependencies between variables (e.g., differences in vegetation height associated with different aspects).

To quantify the amount of variation explained by each physiographic predictor, we used the "relaimpo" package and the option "lmg" [*Gromping*, 2006] in the R statistical computing environment [*R Core Team*, 2013]. This method determines the proportion of variability explained (R^2) by the physiographic variables using sequential R^2 values and accounts for the dependence of the order that predictors were entered into the model by averaging over all possible model orderings. Because we used the same random samples to remove the elevation-based snow depth trend and to perform the multivariate regressions the full variability captured for a site/vegetation class is the sum of the elevation-based R^2 value and the R^2 values of the individual physiographic predictors. We checked for collinearity between covariates by calculating the variance inflation factors which were equal to or slightly above 1 for all regressions, indicating independence between predictors. The residuals for the regressions were normally distributed.

3.3. Interaction of Climate and Physiographic Effects

To evaluate if regional climate characteristics between the sites could explain variability in the effects of physiography on snow depth, we evaluated correlations between the R^2 values of individual physiographic predictors and selected climate metrics. Because of their demonstrated importance on controlling spatial patterns of snow depth we focused on radiation, wind speed, and potential evaporation (a proxy for sublimation). We computed a dimensionless ratio, incoming shortwave to incoming net radiation (SW:NetR$\downarrow$ = shortwave$\downarrow$/(longwave$\downarrow$ + shortwave$\downarrow$)), to evaluate whether the proportioning of incoming radiation between shortwave and longwave was correlated to the relative importance (R^2 values) of aspect (northness). We focused on this metric because radiation is the primary driver of snowpack ablation and therefore is of potential utility for anticipating how climate changes could influence snow distributions. There are a number of climate changes that could affect SW:NetR$\downarrow$ including changes in air temperature, cloudiness, and humidity, and changes to the timing of peak SWE and duration of melt. Changes in air temperature, cloudiness, and specific humidity are all expected/possible with synoptic-scale climate change [*Pepin et al*., 2015]. Furthermore, earlier initiation of melt [e.g., *Musselman et al*., 2017] could reduce SW:NetR$\downarrow$ because sun angles are lower earlier in the year. The SW:NetR$\downarrow$ ratio thus, encapsulates a wide variety of energy effects that are directly relevant to several of our research hypotheses. We computed the ratio (SW:NetR$\downarrow$) for dates before and after the lidar-flights and found that intersite differences in SW:NetR$\downarrow$ were generally consistent, indicating that this ratio helps explain different energy environments among the sites independent of lidar flight timing.

To obtain the meteorological metrics for each site, we used a spatial mask defined by the lidar snow-covered area to extract matching NLDAS pixels and computed a spatial mean for potential evapotranspiration, incoming longwave and shortwave radiation (to compute SW:NetR$\downarrow$), and wind speed. These climate characteristics were tested for correlation (Pearson's r) against the variability in snow depth explained by physiographic predictors (i.e., R^2 values) to evaluate how landscape-vegetation interactions with the atmosphere influenced snow depth patterns across the sites.

Ideally interactions between physiography and climate (e.g., eastness $\times$ wind speed, northness $\times$ SW:NetR$\downarrow$, etc.) and their effects on snow depth would be evaluated in a multivariate regression. The small sample size ($n = 5$) with respect to these interactions obviates a robust regression. Given this limitation, we chose to compute correlation coefficients. Though correlations alone limit inferential power, they could still highlight important atmosphere-landscape-vegetation interactions and their influences on snow depth between sites.

3.4. Distance Between Average Winter Freezing Levels and Snow Volume Percentiles

To gain insights into the potential sensitivity of watershed-scale snow volume to temperature-induced changes in precipitation phase, we computed the distance between the mean winter freezing level (1 November—flight date) and the elevation at which the 25th, 50th, and 75th percentiles of the cumulative snow volume occurred. The freezing levels for each site were determined by solving a linear function, fit to grid cell values of elevation and mean air temperature (1 November—flight date) for a 50 km buffer (i.e., 3 $\times$ 3 grid cell neighborhood) around each site's snow-covered area, for the 0°C elevation. Note that any melt on or near the flight date could reduce the accuracy of this metric. This metric may be improved by refined estimates such as only using temperatures on storm-days to compute average winter temperature [e.g., *Klos et al*., 2014], or by tracking changes in dew point temperature with elevation during storms to compute rain-snow transitions [*Marks et al*., 2013]. Evaluating how spatial variability in snow density [e.g., *Wetlaufer et al*., 2017] affects the utility of this metric is also an important consideration that is not tested here.

Snow volume distributions were calculated by taking the product of snow depth and the area of each pixel (9 m^2) and computing the mean snow volume for each elevation bin. We also used the snow volume and area-elevation distributions (i.e., hypsometric distributions) to evaluate "geometric-based" arguments that the temperature sensitivity of snowpack is related to catchment hypsometry and rates of freezing level increase [*Casola et al*., 2009; *Klos et al*., 2014; *Tennant el al*., 2015a]. To test how well the hypsometry (i.e., elevation distributions) of the snow-covered areas at each of the sites reflected the elevations of greatest snow storage, we computed a similarity index (*SI*) [*Agresti*, 1996]:

$$SI = \left[1 - \left(\frac{1}{2}\left(\sum_{i=1}^{N} |A_i - S_i|\right)\right)\right] \times 100 \quad (1)$$

where A_i is the fractional amount of area and S_i is the fractional amount of snow volume at the ith elevation bin and N is the total number of elevation bins. The SI score measures the similarity between distributions, 0% indicates no overlap and 100% identical area (A_i) and snow volume (S_i) distributions. Area and snow volume were normalized by their respective ranges before computing the SI scores.

4. Critical Zone Observatory Study Sites

4.1. Overview

The CZO study sites differ in their vegetation characteristics, topography, and regional climate and provide a unique opportunity to evaluate how physiography and climate influence regional-scale snow depth patterns across a range of conditions (Table 1). Winter precipitation from 1 November until the respective snow-on flight dates ranged from 58 cm (JRB) to 243 cm (KREW) and mean winter temperatures were as low as −5.4°C (BCW) to as warm as 2.2°C (KREW). Most of the sites cover a relatively large range of elevations; therefore, precipitation and SWE within a given site can be quite variable between low and high elevations. For example, RCEW has the longest meteorological records, which show that average annual precipitation has ranged from 24 cm (1188 m) up to 112 cm (2170 m) [*Hanson*, 2001] and average annual peak SWE from 22 cm (1743 m) to 72 cm (2167 m) [*Marks et al*., 2001]. Because of the sites' relief and varying climatic characteristics, vegetation cover is also variable. For example, WOLV has an extensive alpine zone comprising 53% of its area whereas 89% of RCEW is shrub-covered. The site characteristics and lidar snow depth errors are described in detail in the following sections 4.2–4.5.

4.2. Boulder Creek CZO

The Boulder Creek CZO is located within the Boulder Creek Watershed (BCW) in the Rocky Mountains of Colorado, USA (Figure 1). Lidar snow-covered surveys for BCW were conducted on 5 May 2010 and 25 May 2010. Because melt occurred between 5 and 25 May, we only used snow depths from the 5 May flight as these values better represented snow depths near peak accumulation. The average RMSE ($n = 21$) of lidar-derived snow depths for BCW was 16 cm. Average winter temperature and total precipitation were −5.4°C and 85 cm, respectively, and the average wind speed was 6.5 m/s (Table 1). Vegetation cover in BCW included forest (35%), shrub (38%), and alpine (27%) areas (Table 1). Forest were dominated by evergreen

Table 1. Meteorological, Topographic, and Vegetation Characteristics of the Study Sites[a]

Site	BCW	JRB	RCEW	KREW	WOLV
Snow-covered area (km^2)	261	294	75	18	59
Snow-off flight date	21–26 Aug 2010	29 Jun to 8 Jul 2010	10–18 Nov 2007	5–15 Aug 2010	5–15 Aug 2010
Snow-on flight date	5 May 2010	1 Apr 2010	19 Mar 2009	20 Mar 2010	21–22 Mar 2010
Mean lidar snow depth (cm)	34	71	114	146	276
Lidar snow depth RMSE (cm)	16	22	27	24.5	23
% pixels with no snow cover	11	8	14	2	0.35
Average winter temperature (°C)	−5.4 ± 2.6	−3.3 ± 0.3	0.1 ± 1.5	2.2	−1.6 ± 3.5
Average winter potential ET (mm/d)	1.7 ± 0.37	1.6 ± 0.03	1.9 ± 0.05	1.5	1.4 ± 0.13
Average winter SW:NetR↓	0.43	0.44	0.33	0.36	0.39
Average winter wind speed (m/s)	6.5 ± 0.4	3.9 ± 0.1	3.9 ± 0.2	1.6	2.7 ± 0.9
Total winter precipitation (cm)	85 ± 25	58 ± 4	64 ± 26	243	174 ± 34
Mean elevation (m)	3043	2702	1843	1846	2844
Relief (m)	1730	1187	906	829	1704
Tree line elevation (m)	3298			2081	2916
Alpine (%)	27			1	53
Forest (%)	35	51	11	60	19
Shrub (%)	38	49	89	39	28
Mean vegetation height forest (m)	6.2	10.4	6.2	13.3	14.5
COV vegetation height (%)	49	53	77	65	69

[a]The flight dates, lidar mean snow depth and RMSE for BCW, JRB, KREW, and WOLV are from *Harpold et al*. [2014a] and for RCEW are from *Tinkham et al*. [2014]. The lidar mean snow depth is the mean for the field surveys not the full snow-covered area. COV is the coefficient of variation. Winter refers to the period 1 November until each sites respective flight date. The climate metrics report the spatial mean ± one standard deviation except KREW which was covered by one NLDAS pixel.

species and were composed of ponderosa pine (*Pinus ponderosa*), subalpine fir (*Abies lasiocarpa*), Engelman spruce (*Picea engelmannii*), and lodgepole pine (*Pinus contorta*) [*Harpold et al*., 2014a].

4.3. Jemez River Basin-Santa Catalina Mountain CZO

The Jemez River Basin (JRB), part of the Jemez River Basin-Santa Catalina Mountain CZO, is located in northern New Mexico at the southern end of the Rocky Mountains New Mexico, USA (Figure 1). The snow-covered LiDAR flight occurred on 1 April 2010 and had a RMSE ($n = 9$) of 22 cm. The average winter temperature and precipitation at JRB were −3.3°C and 58 cm, respectively, and average wind speeds were 3.9 m/s (Table 1). Vegetation cover at JRB included forest (51%) and shrub (49%; Table 1). Like BCW, forest-cover was composed of evergreen species, Douglas-fir (*Pseudotsuga menziesii*), white fir (*Abies concolor*), blue spruce (*Picea pungens*), southwestern white pine (*Pinus strobiformis*), limber pine (*Pinus flexilis*), and ponderosa pine but also included a limited number of aspen groves (*Populus tremuloides*) [*Harpold et al*., 2014a].

4.4. Reynolds Creek CZO

The Reynolds Creek CZO is located in the Reynolds Creek Experimental Watershed (RCEW) at the northern edge of the Northern Basin and Range in southwestern Idaho, USA (Figure 1). The snow-covered flight occurred on 19 March 2009 [*Shrestha*, 2016], with an average RMSE ($n = 544$) of 27 cm [*Tinkham et al*., 2014]. The average winter temperature and precipitation at RCEW were 0.1°C and 64 cm, respectively, and the average wind speed was 3.9 m/s (Table 1). Vegetation at RCEW was dominated by shrub (89%) with small areas of isolated forest (11%) that occurred in topographically sheltered areas (Table 1). The forest stands were mostly homogenous and composed of either aspen, subalpine fir, or Douglas fir [*Tinkham et al*., 2014; *Slaughter et al*., 2001].

4.5. Southern Sierra CZO

4.5.1. Kings River Experimental Watershed

The Kings River Experimental Watershed (KREW) is part of the Southern Sierra CZO and is located in the Sierra Nevada, California, USA (Figure 1). The snow-covered lidar flight [*Guo* and *Bales*, 2012] occurred on 20 March 2010 with an average snow depth RMSE ($n = 18$) of 24.5 cm. The average winter temperature and precipitation were 2.2°C and 243 cm, respectively, and wind speeds averaged 1.6 m/s (Table 1). Land cover at KREW was dominated by forest (60%), with shrubs covering the majority (39%) of the remaining area (Table 1). The highest elevations of the KREW were primarily rock outcrops with limited vegetation cover, thus the upper 1% of snow-covered area of KREW was classified as alpine (Table 1). Forest-cover was a mix of conifer forests of white fir, Jeffrey pine (*Pinus jeffreyi*), ponderosa pine, sugar pine (*Pinus lambertiana*), incense-cedar (*Calocedrus decurrens*), and a minor component of lodgepole pine with isolated California black oak (*Quercus kelloggii*) interspersed in a limited number of locations [*Harpold et al*., 2014a].

4.5.2. Wolverton Basin

The Wolverton (WOLV) basin is also part of the Southern Sierra Critical Zone Observatory (Figure 1). The snow-covered lidar flights occurred on 21 and 22 March 2010 [*Anderson et al*., 2012; *Guo and Bales*, 2012], with an overall RMSE ($n = 12$) of 23 cm. The average winter temperature and precipitation were −1.6°C and 174 cm, respectively and wind speeds averaged 2.7 m/s (Table 1). WOLV had the largest alpine area (53%) and slightly more shrub cover (28%) than forest (19%; Table 1). Forests at WOLV consisted of red fir (*Abies magnifica*), lodgepole pine, western white pine (*Pinus monticola*), incense-cedar, Jeffrey pine, red fir, western white pine, and lodgepole pine [*Harpold et al*., 2014a].

5. Results

5.1. Snow Depth-Elevation Relationships

Mean snow depths generally increased with elevation despite differences in topography, vegetation, and regional climate between the sites (Figure 2a). Though the overall trends were positive (see median dS/dE values Table 2), the relationships were notably nonlinear and snow depths exhibited localized declines, zero increase, or rapid rates of increase (Figure 2b). At the highest elevations of three of the sites, frequent or continuous declines in snow depth were observed (BCW, RCEW, and WOLV, Figure 2a). Median rates of snow depth increase with elevation ranged from 0.64 cm/100 m up to 1.03 cm/100 m (Table 2) and the site to site variability in dS/dE with elevation (black lines Figure 2b) was reflected in the variance and kurtosis of the dS/dE distributions (Figure 3).

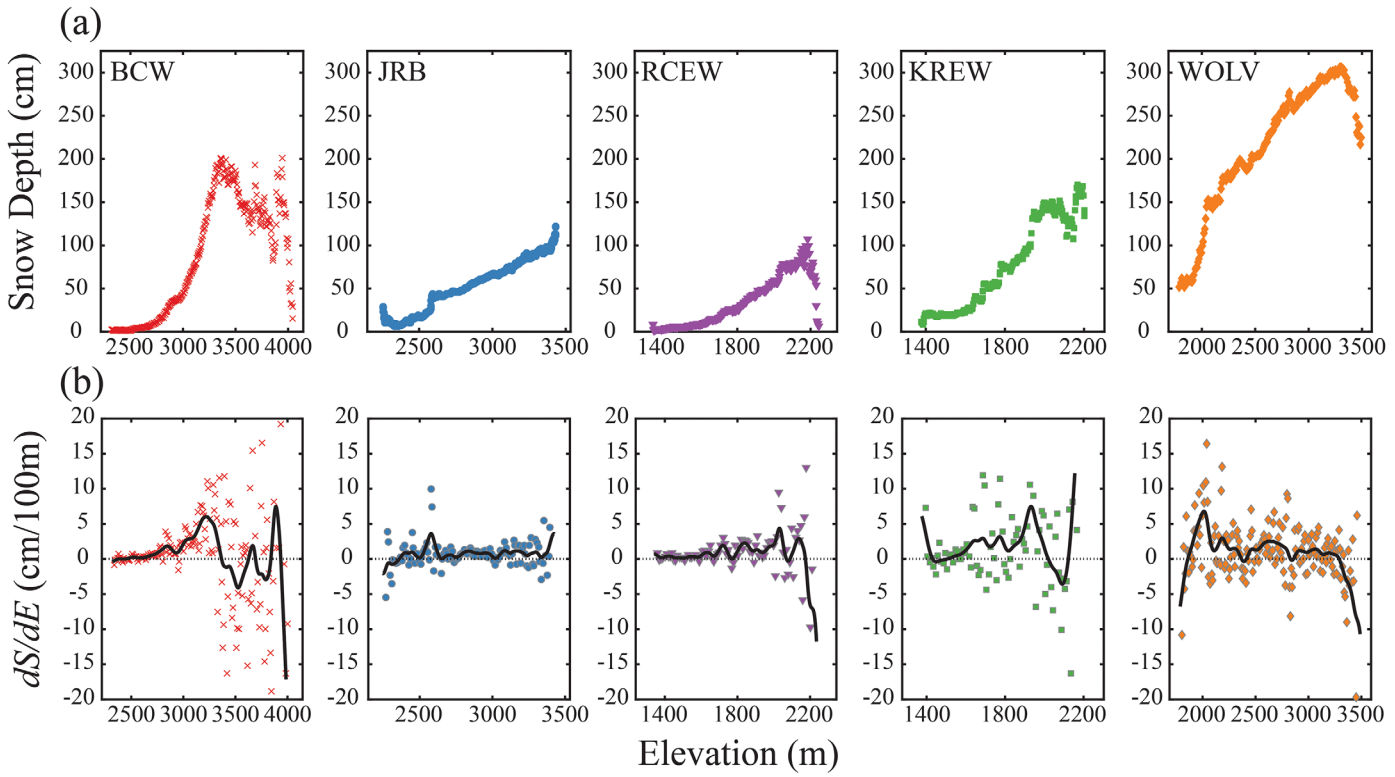

Figure 2. (a) Mean snow depths plotted against elevation and (b) the first derivative of mean snow depth and elevation (*dS/dE*) with smoothing splines (black lines) to reveal the general trends. The *x* axes are site specific to better reveal the snow depth-elevation relationships and their derivatives. The *y* axes in Figure 2b are truncated for BCW, KREW, and WOLV, and exclude 4%, <1%, and 1%, respectively, of *dS/dE* values. Maximum and minimum *dS/dE* values are summarized in Table 2.

5.2. Effects of Vegetation and Aspect on Snow Depth

The ANOVA tests demonstrate that aspect, vegetation class, and their interaction (aspect × vegetation class) resulted in significant differences in mean snow depth (Figure 4). The effect of aspect was significant at all sites and grouping by vegetation class was also significant except at BCW and RCEW (Table 3). The statistical significance of the interaction term (aspect × vegetation class; Table 3) at all sites indicates that the influence of vegetation on snow depth varied as a function of aspect. Pairwise comparisons based on Tukey's HSD test show that mean snow depths for open (alpine and shrub) northern aspects were greater than mean values for all aspects in forested areas and southern aspects in alpine and shrub areas (Figure 4). BCW and RCEW were an exception to this pattern where southeast aspects had mean values that were higher than expected (Figure 4); these sites also had the highest westerly wind speeds (Table 1). At RCEW this result may be affected by a high RMSE of LiDAR derived snow depths in shrub areas [*Tinkham et al.*, 2014], but also may reflect greater accumulations on small patches of southeast-facing land that occur near slope breaks where flow separation of westerly winds is likely to occur [e.g., *Prasad et al.*, 2001]. Greater accumulations on BCW's southeast aspects may also reflect avalanching [e.g., *Erickson et al.*, 2005].

5.3. Snow Depth Variability Explained by Elevation, Aspect, and Vegetation

The total variability (R^2) in snow depth captured by the multivariate regression models was generally high in forest (22–99%) and shrub areas (36–97%) but declined in alpine zones (16–70%; Table 4). The elevation-

Table 2. The Minimum, Median (With 95% Confidence Interval), and Maximum Values for the First Derivative of Snow Depth and Elevation (*dS/dE*) Expressed as cm/100 m

dS/dE (cm/100 m)	BCW	JRB	RCEW	KREW	WOLV
Min	−33	−5	−10	−17	−25
Median	0.73 ± 0.2	0.71 ± 0.05	0.64 ± 0.1	0.70 ± 0.2	1.03 ± 0.4
Max	49	10	13	40	16

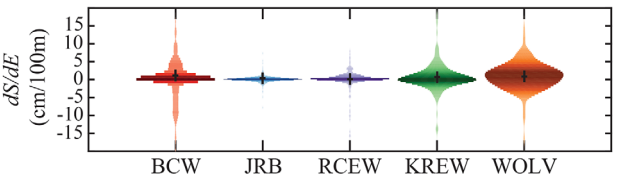

Figure 3. Distributions of the derivative of mean snow depth and elevation (*dS/dE*) for the study sites. The median *dS/dE* are displayed (black crosses) and the width and color-shading on the violin plots show the relative density of *dS/dE* values; wider regions/darker colors indicate a greater number of observations. Values >20 cm/100 m and <−20 cm/100 m were omitted for BCW, KREW, and WOLV to better display the distributions, and exclude 4%, <1%, and 1%, respectively, of the *dS/dE* values. See Table 2 for confidence intervals on medians and summary statistics.

based snow depth trends were generally the best predictors in forests and shrub areas where they, respectively, captured 16–79% and 21–57% of the variability in snow depth (Table 4). In alpine areas, the relationships between elevation and snow depth were less consistent (Figure 2a) and the elevation-based snow depth trends captured <0.1–6% of the total variability (Table 4). These findings generally agree with previous efforts that report dependencies of snow depth on elevation [e.g., *Grünewald et al.*, 2013; *Kirchner et al.*, 2014; *Walters et al.*, 2014; *Zheng et al.*, 2016].

The aspect-based metrics (northness and eastness), were the most important predictors of snow depths in alpine zones where northness captured between 1% and 35% of the variability and eastness 3% to 10% (Table 4). Northness was also an important predictor of snow depth in forest and shrub areas, explaining 1–35% of the variability in forests and 4–37% in shrub areas. Eastness was important in RCEW's shrub area and BCW's alpine area where westerly wind speeds were predominant.

5.4. Relationships Between Physiographic Effects and Regional Climate

5.4.1. Alpine Areas

In the alpine areas (only present in BCW, KREW, and WOLV), the percent of variability in snow depth explained by northness and eastness exhibited significant correlations with wind speed and potential ET, respectively. The variability in snow depth explained by northness exhibited an inverse relationship with wind speed ($r = -0.99$, $n = 3$; Figure 5a). At KREW and WOLV, wind speeds were lower, and northness was positively related to snow depth and captured 24% and 34% of its variability, respectively. At BCW wind speeds were higher and northness only explained 1% of the variability in snow depth. The other significant correlation in alpine areas was a positive relationship between potential ET and the variability in snow depth captured by eastness ($r = 0.99$, $n = 3$; Figure 5b). Eastness explained 10% of snow depth variability in BCW's alpine zone where wind speeds and potential ET were highest.

5.4.2. Forest Areas

In forests, the variation in snow depth explained by northness was positively correlated with the ratio of incoming shortwave to incoming radiation (SW:NetR↓; $r = 0.86$, $n = 5$; Figure 5c). The importance of northness as a snow depth predictor in forests peaked at BCW and JRB, where SW:NetR↓ approached 0.5. A negative correlation was observed between the variability in snow depth explained by vegetation height and SW:NetR↓ ($r = -0.85$, $n = 5$; Figure 5d). Vegetation height was correlated more strongly with snow depth at RCEW, KREW, and WOLV where SW:NetR↓ values were lower.

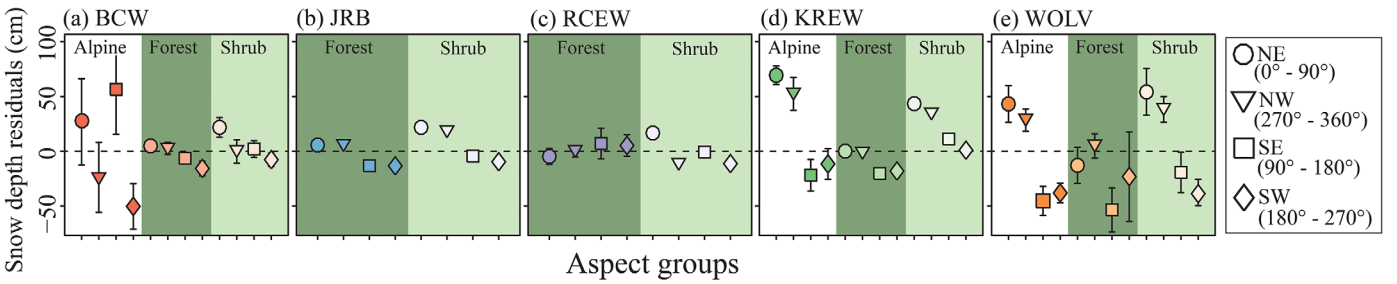

Figure 4. Comparison of mean values for snow depth residuals (section 3.1.1). (a–e) Residuals are grouped by 90° aspect quadrants (see legend) for alpine (white background), forest (dark green), and shrub (light green) vegetation classes for the study sites. The symbols show aspect-dependent means for each vegetation class. The vertical lines on the symbols show 95% comparison intervals from a Tukey's HSD test. If intervals do not overlap, the means are statistically different. Mean values that are greater or less than expected, based on a site's elevation-based snow depth trend (section 3.1.1), plot above and below the dashed zero lines, respectively.

Table 3. *p* Values for *F* Test in ANOVA Revealed That Grouping by Aspect (NE, 0–90°, SE, 90–180°, SW 180–270°, NW 270–360°) Resulted in Significant Differences (*p* value < 0.05) in Mean Snow Depth at all Sites[a]

	BCW	JRB	RCEW	KREW	WOLV
Aspect *p* value	<0.0001	<0.0001	<0.0001	<0.0001	<0.0001
Vegetation *p* value	$0.07^{n/s}$	<0.0001	$0.37^{n/s}$	<0.0001	0.001
Aspect × vegetation *p* value	<0.0001	0.005	<0.0001	<0.0001	0.02

[a]Grouping by vegetation class (forest, shrub, and if present alpine) resulted in significant differences at all sites except BCW and RCEW (*p* values marked with n/s superscript to indicate nonsignificance). The interaction of aspect and vegetation class was significant at all sites.

5.4.3. Shrub Areas

In shrub areas, significant correlations between the percent of snow depth variability explained by northness and the ratio of SW:NetR↓ were again identified ($r = 0.88$, $n = 5$; Figure 5e). Northness explained a greater amount of snow depth variability (11–37%) in shrub areas than in forests, and the correlations between northness and snow depth were significant at all sites. The importance of northness as a snow depth predictor for shrub areas also peaked at BCW and JRB where SW:NetR↓ was highest.

The maximum correlation (*r*) between the climate metrics (potential evapotranspiration, SW:NetR↓, and wind speed) across the sites was 0.53 ($n = 5$), thus we expect that each of these factors represents at least some unique information regarding climate-landscape-vegetation interactions. Longer-term feedbacks between geology, soils, and climate also likely influence the correlations presented here, however, teasing apart these effects is beyond the scope of this work.

5.5. Distances Between Average Winter Freezing Levels and Catchment Snow-Volume Percentiles

The sites with the smallest vertical distances between their mean winter freezing levels and their elevations of 50% of cumulative snow volume were KREW and RCEW (Table 5). These sites had the lowest mean elevations of all the surveyed areas (Table 1). We also found that the range over which the 25th to 50th % of cumulative snow volume was stored was quite variable, ranging from 152 m at KREW up to 568 m at WOLV and that the snow-covered hypsometries were generally good predictors of snow volume except at BCW and RCEW (See *SI* scores Figure 6).

6. Discussion

6.1. Watershed Snowpack Controls

6.1.1. Evaluation of Study Hypotheses (H1–H4)

Decades of field observations and modeling work have shown landscape structure, expressed by the joint distribution of elevation, topography, and vegetation, to be a major control on energy and water partitioning and spatial patterns of snowpack [e.g., *Adams*, 1976; *Blöschl et al.*, 1991a, 1991b; *Elder et al.*, 1991; *U.S.*

Table 4. Variability in Snow Depth Explained (R^2) by the Elevation-Based Snow Depth Trends, the Physiographic Predictors, and the Sum of the Elevation-Based Snow Depth Trends and the Physiographic Predictors (total R^2) in Alpine, Forest, and Shrub Areas for Each Study Site

			Physiographic Predictors R^2 (%)					
CZO		Elevation-Based Snow Depth Trend R^2 (%)	Eastness	Northness	Slope	Vegetation Height	Physiographic Total	Total R^2 (%)
BCW	Alpine	<0.1	10	1	5	0	16	16
	Forest	79	2	15	3	<0.1	20	99
	Shrub	57	5	27	2	1	35	92
JRB	Forest	34	2	35	3	0	40	74
	Shrub	24	<0.1	37	6	3	46	70
RCEW	Forest	16	<0.1	1	<0.1	5	6	22
	Shrub	21	4	4	1	6	15	36
	Alpine	6	6	34	22	2	64	70
KREW	Forest	41	1	4	2	6	13	54
	Shrub	54	1	21	18	3	43	97
	Alpine	<0.1	3	24	2	0	29	29
WOLV	Forest	64	2	12	7	3	24	88
	Shrub	34	<0.1	33	9	0	42	76

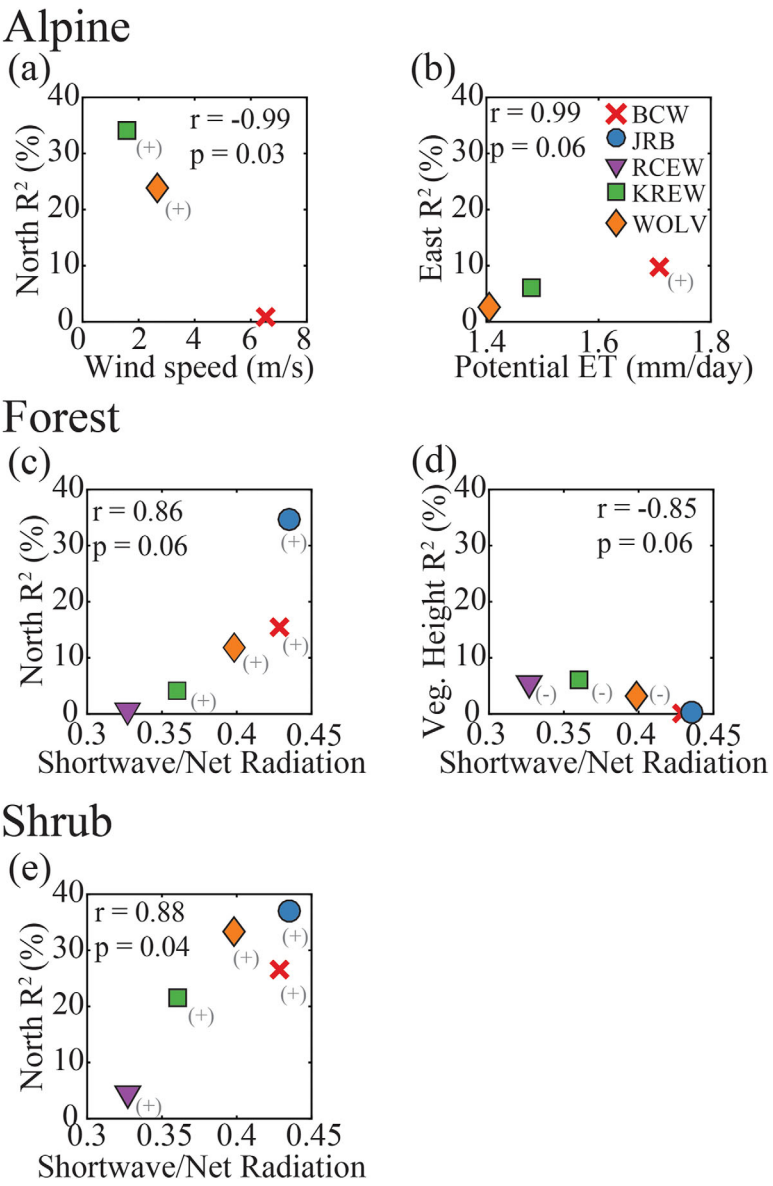

Figure 5. Correlations between the variability in snow depth explained (R^2) by the physiographic predictors and selected climate metrics for (a and b) alpine, (c and d) forest, and (e) shrub areas for the study sites (legend in Figure 5b applies to all panels). The Pearson correlation coefficients (r) and their p values (p) for the relationships between the climate metrics (x axes) and the physiographic predictors (y axes) are displayed in each plot. The sign (+ or −) next to the symbols shows the direction of the relationship between the physiographic predictor (y axis) and snow depth at each site. The sign is only plotted when the relationship between the physiographic predictor and snow depth is significant (i.e., p value < 0.05).

Table 5. Mean Winter Freezing Levels (From November to Respective Flight Dates; See Table 1), Vertical Distances Between Freezing Levels and the 25th, 50th, and 75th Percentile of Cumulative Snow Volume, and the Elevation Range Between the 25th and 75th Percentiles of Cumulative Snow Volume for the Study Sites

		BCW	JRB	RCEW	KREW	WOLV
Freezing level elevation (m)		2027	1919	1685	2050	2050
Vertical distance between freezing level and elevation of cumulative snow volume	25%	1159	748	177	−214	627
	50%	1314	842	313	−105	1006
(SV) percentiles:	75%	1474	978	400	−62	1195
SV_{75}–SV_{25} (m)		314	230	222	152	568

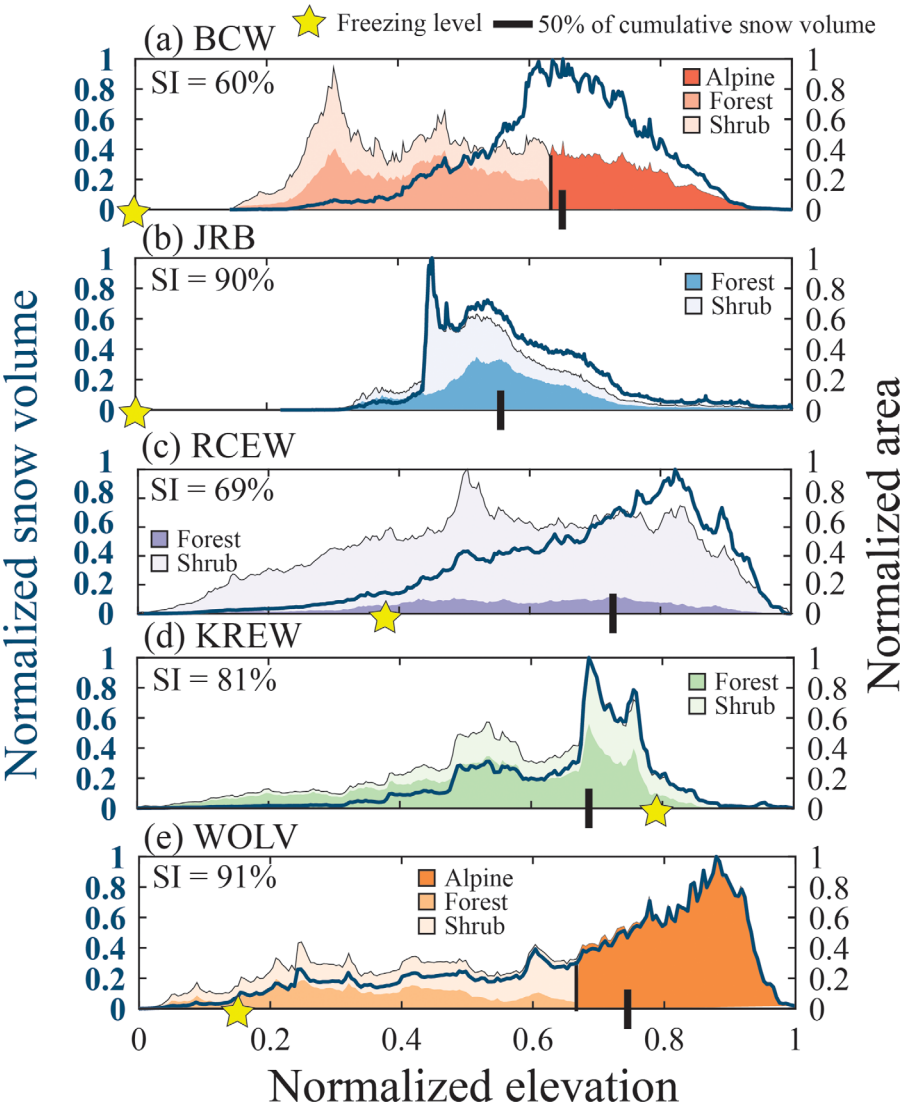

Figure 6. (a–e) Distributions of normalized snow volume (primary *y* axes), area (secondary *y* axes), and vegetation class (inset legends) as a function of normalized elevation for the study sites. The mean winter freezing level (stars), elevation of the 50th percentile of cumulative snow volume (thick vertical line), and the similarity indices (*SI*) are also plotted for each site. See Table 5 for nonnormalized distances between freezing levels and the elevations of snow volume percentiles.

Army Corps of Engineers, 1956]. The analyses presented here offer new insights because they were based on high-resolution (3 m) airborne lidar surveys that extended observations beyond existing meteorological stations within each region (e.g., Figure 7). Furthermore, this study provides a novel synthesis of the effects of aspect and vegetation on snow depth at regional scales (up to 290 km^2) across diverse physiographic and climatic settings (Figure 1). We use our results to evaluate H1–H4 and compare our findings to previous field and modeling-based studies.

Our first hypothesis (H1) was that elevation-driven effects would be an important control on snow depth variability across all the sites, which we found to be true (Table 4). This agrees with fundamental expectations that "orographic effects on precipitating clouds" [*Houze*, 2012] often result in greater precipitation at higher elevations where temperatures are cooler and more snowpack can accumulate. Field and modeling work at or nearby the study sites used here (Figure 1) have demonstrated strong orographic precipitation gradients [*Dettinger et al.*, 2004; *Girotto et al.*, 2014; *Hanson*, 2001; *Hay and McCabe*, 1998; *Kirchner et al.*, 2014; *Knowles et al.*, 2015; *Lundquist et al.*, 2008, 2010; *Marks et al.*, 2001; *Rhea*, 1977; *Tarboton et al.*, 2001] and in particular, studies from the Sierra Nevada have demonstrated the importance of wind direction,

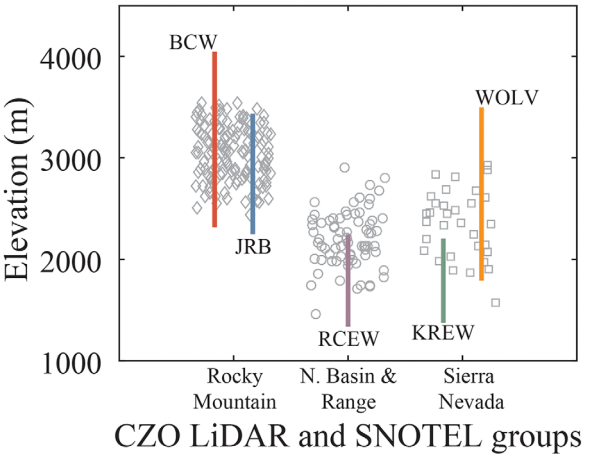

Figure 7. Comparison of the range of elevations measured during the lidar flights (vertical lines) and the elevations of SNOTEL stations in Rocky Mountain (Colorado and New Mexico stations, diamonds), northern Basin and Range (Idaho $< 44°$ latitude and Nevada $> 40°$ latitude stations, circles), and Sierra Nevada (California stations, squares). At all locations, the lidar snow-on flights extend the range of snow depth measurement to higher (except RCEW) and/or lower elevations.

wind speed, and the height of mountain-parallel barrier jets on controlling increases in precipitation with elevation [*Dettinger et al*., 2004; *Lundquist et al*., 2010].

We also found (H2) that snow depths in different vegetation classes (i.e., alpine, forest, and shrub) exhibited statistically significant differences (Figure 4 and Table 3). Because we removed the elevation-based snow depth trends before performing ANOVA, these results likely reflect effects related to differences in ablation, interception, redistribution, and shading between the vegetation classes. The general finding that open areas (alpine and shrub in this study) accumulated greater snow depths because of reduced interception is supported by numerous field and modeling studies [*Broxton et al*., 2015; *Gelfan et al*., 2004; *Golding and Swanson*, 1978; *Hubbart et al*., 2015; *Knowles et al*., 2015; *Tinkham et al*., 2014]. Furthermore, compilation of field observations from 65 sites across North America demonstrated a strong relationship showing decreased snow depths with increased forest-cover [*Varhola et al*., 2010], pointing to the role of canopy interception in reducing snow depths in forests. The results presented here demonstrate that these same patterns of greater snow depths in open vs. forested areas are evident at the watershed-scale (Figure 4).

(H3) Numerous studies have demonstrated that in the absence of tall vegetation the importance of aspect and slope (proxies for solar radiation and wind-shelter) are dominant controls on snow accumulation and redistribution. Here, we contribute further by evaluating how wind speed and the partitioning of incoming radiation between shortwave and longwave (SW:NetR↓) affected the variability in snow depth captured by northness and eastness. We hypothesized (H3) that slope and aspect (northness and eastness) would capture more snow depth variability at sites with greater shortwave inputs (high SW:NetR↓) and high wind speeds. We found the importance of northness peaked in forest and shrub areas at RM sites (Table 4) where the ratio of incoming shortwave to incoming total radiation (SW:NetR↓) was highest (Table 1), which supports H3. We also found that eastness captured the greatest amount of variability in snow depth in open areas in BCW's alpine and RCEW's shrub areas, which were the sites with the highest westerly wind speeds (Tables 1 and 4). The importance of sheltered aspects for controlling patterns of wind-blown snow deposition have been demonstrated by several field and modeling studies conducted in BCW's alpine and RCEW's shrub area [*Erickson et al*., 2005; *Knowles et al*., 2015; *Luce et al*. 1998; *Marks et al*., 2003; *Tarboton et al*. 2001; *Winstral and Marks*, 2002; *Winstral et al*., 2013].

We also hypothesized (H4) that shading by tall vegetation in forests would be more important at sites with greater shortwave inputs (i.e., higher SW:NetR↓). Interestingly, the variability in snow depth captured by vegetation height was greatest at sites with greater longwave inputs (Figure 5d; Tables 1 and 4), which contrasted our expectation. We posit that at sites with greater longwave inputs (RCEW, KREW, and WOLV), the negative relationships between snow depth and vegetation height were caused by interception losses and longwave-driven ablation beneath the canopy. This idea agrees with the results of *Lundquist et* al. [2013] who demonstrated that longwave-driven ablation was an important control on snow losses in forest sites where average winter temperature was $>\sim 1°C$. At sites with greater shortwave inputs (BCW and JRB), tall vegetation in forests likely acted to intercept snowfall but also to shade snowpack and reduce ablation; thus the effects counteracted and little variability in snow depth was captured by vegetation height in forest areas at RM sites (BCW, JRB, Table 4). The findings at BCW and JRB agree with field results from nearby areas that showed greater accumulation in open versus under canopy areas at the tree-scale, but no overall increases in forest snowpack following fire and pine beetle-caused stand-scale canopy loss [*Bierdman et al*., 2014; *Harpold et al*., 2014b].

Using high-resolution observations of snow depth, topography, and vegetation combined with reanalysis climate products, we were able to evaluate a number of hypotheses (H1–H4). We have high confidence in our evaluations of H1 and H2, as they were based on robust analyses of lidar-derived snow depth, vegetation, and topography where sample sizes were large and all statistical assumptions were met. Because H3 and H4 were not evaluated in the context of a formal statistical test (see section 3.3), further corroboration is needed to support our interpretations.

6.2. Potential Snowpack Sensitivities

6.2.1. A Proposed Measure of Watershed Snowpack Sensitivity to Shifts From Snow to Rain

Estimating watershed snowpack sensitivity to temperature-driven shifts from snow to rain [e.g., *Luce et al*., 2014] is necessary for predicting potential responses of streamflow to changes in snowpack amount and melt timing [*Barnhart et al*., 2016; *Berghuijs et al*., 2014; *Ryberg et al*., 2015; *Tennant et al*., 2015b; *Wang et al*., 2016]. We leveraged the unprecedented ability of airborne lidar surveys to estimate watershed snow volume distributions to develop a simple metric—the distance between the average winter freezing level and the elevation of the 50th% of cumulative snow volume (section 3.4)—as a proposed measure of the sensitivity of watershed snow volume to shifts from snow to rain (Figure 6).

Small vertical distances between freezing levels and the elevations with significant snow volume at KREW and RCEW indicate that these sites currently have the highest sensitivity to shifts from snow to rain (Table 5). KREW had a negative distance between its freezing level and zone(s) of significant snow volume which suggests that its snowpack may experience frequent rainfall and melt throughout winter months. Indeed, wet, unfrozen subnivean soil and soil moisture increases during winter months have been documented at Southern Sierra sites located in or near KREW [*Bales et al*., 2011; *Harpold et al*., 2014c].

Also, the similarity between the snow volume and elevation distributions was generally high (60–91%; mean = 78%; Figure 6) indicating that the hypsometry of the sites' snow-covered areas were good predictors of where snow volume was greatest. These findings support "geometry-based" arguments that knowledge of snow volume—elevation distributions and freezing levels can help predict potential responses of mountain snowpack to warming over regional extents [*Casola et al*., 2009; *Klos et al*., 2014; *Minder*, 2010; *Tennant et al*., 2015a; *Wayand et al*., 2015]. The utility of the hypsometric approach, expanded on here, is also supported by 45 years of temperature, rainfall, and snowfall measurements from RCEW demonstrating elevation-dependent warming and shifts from snow to rain [*Nayak et al*., 2010].

Differences between the sites in the vertical distances between freezing levels and snow volume percentiles (Table 5) and the spatial variability in snow volume as related to catchment hypsometry (Figure 6) suggest the potential for differential responses to regional warming and shifts from snow to rain. The results (Table 5 and Figure 6) presented here suggest that airborne lidar estimates of snow volume and regional temperatures can help identify watersheds that are sensitive or more resistant to shifts from snow to rain.

6.2.2. Potential Sensitivities of Snowpack to Climate and Vegetation Changes

In the following sections, we highlight a series of hypotheses that help inform potential watershed-scale snowpack sensitivities to shifts in climate or vegetation in alpine, forest, and shrub areas across these western U.S. sites. While the hypotheses below are supported by our results and existing work, further validation is needed given the small sample size ($n = 5$) and uncertainty regarding the relationships between climate characteristics and the importance of physiographic proxies as snow depth controls (Figure 5).

6.2.2.1. Potential Sensitivities of Snow Depth to Changes in Wind Speed

In alpine settings where westerlies dominate, global wind stilling [*McVicar et al*., 2012; *Luce et al*., 2013] could impact snow depth patterns by reducing snow redistribution from western to eastern slopes and could increase the importance of storage on northern aspects. This hypothesis is supported by the observation that eastness captured the greatest variability in snow depth in BCW's alpine zone (Table 4) where wind speeds were the highest (Table 1) and by the fact that northness explained much more variability in snow depth at KREW and WOLV where wind speeds were lower (Figure 5a). The low variability of snow depth captured by northness in BCW's alpine zone is especially surprising given its high SW:NetR$\downarrow$ (Table 1). This observation, coupled with the ANOVA and regression results, emphasize the importance of snow storage on eastern slopes. These results also agree with findings from a study conducted in BCW's alpine zone

[*Erickson et al*., 2005] that demonstrated that wind sheltering had the largest effect on spatial snow depth patterns.

Wind stilling may also increase the importance of alpine snowpack storage by reducing wind-blown sublimation, which has been shown to be a major driver of alpine water losses [*Hood et al*., 1999; *MacDonald et al*., 2010; *Marks and Dozier*, 1992; *Knowles et al*. 2015]. Because the influence of wind falls precipitously with increases in forest-cover, tree line shifts [*Goulden and Bales*, 2014; *Salzer et al*., 2009] could also be important by limiting zones with significant redistribution and high rates of wind-blown sublimation to higher elevations. Furthermore, reduced wind speeds could have even larger-scale effects by decreasing orographic precipitation enhancement. For example, *Luce et al*. [2013] demonstrated that declines in winter precipitation (November–March) at high elevation meteorological stations were likely caused by decreases in lower troposphere wind speeds and suggested that reduced orographic precipitation enhancement was the primary driver of observed streamflow declines in the Pacific Northwest.

6.2.2.2. Potential Sensitivities of Snow Depth to Shifts in SW:NetR↓ in Forest and Shrub Areas

Increases in downwelling longwave radiation and shifts to lower SW:NetR↓ are likely to occur with increases in air temperature, cloudiness, specific humidity, and earlier peak SWE (section 3.3). While aspect was generally important at all of the sites, the higher SW:NetR↓ (Table 1), and greater importance of aspect (Table 4) at RM sites suggest that they may be more responsive to potential decreases in SW:NetR↓ caused by warming or changes in atmospheric water vapor. If SW:NetR↓ lowers then the importance of aspect could decrease because of more spatially uniform ablation. However, this effect could be limited by a positive feedback where earlier melt on south-facing slopes (due to less cold content and greater energy inputs) enhances the effects of aspect and offset more spatially uniform ablation.

6.2.2.3. Potential Sensitivities of Snow Depth to Vegetation Changes in Forest Areas

Differential sensitivity of snowpack to vegetation change is likely due to the varying importance of vegetation as a snow depth predictor across the sites (Table 4). Vegetation height captured the greatest amount of snow depth variability (up to 6%) at RCEW, KREW, and WOLV where it was negatively correlated with snow depth which we assume primarily reflects canopy interception losses. Given the large amounts of forested area and the importance of vegetation height as a predictor at KREW (Tables 1 and 4), Sierra sites could be the most responsive to canopy thinning.

7. Conclusion

In this study, we utilized regional-scale airborne lidar surveys (18–294 km^2) of snow depth, topography, and vegetation to evaluate how differences in climate and physiography influenced watershed-level snow depth distributions at five mountainous sites in western North America. The variability in snow depth explained by aspect, elevation, and vegetation height varied between vegetation class (alpine, forest, and shrub) and with regional climate. Snow depth increase with elevation was the dominant trend at all sites, however, these relationships were notably nonlinear and snow depth exhibited continuous declines at the highest elevations of three of the five sites. Elevation and aspect captured the greatest amount of variability in snow depth in forest and shrub areas, however, in alpine areas only aspect (northness and eastness) was important. In forest and shrub areas, the importance of aspect and vegetation height varied with changes in the ratio of incoming shortwave to incoming net radiation (SW:NetR↓). Aspect peaked in importance at sites with high SW:NetR↓ and forest vegetation height explained more snow depth variability at warmer sites with lower SW:NetR↓.

The importance of elevation and aspect at all sites suggest that warming and changes in SW:NetR↓ could have widespread and varied effects on western U.S snowpacks. Given the importance of elevation and the high certainty of future warming we proposed a new metric, the distance between the average winter freezing level and the elevation of the 50th% of cumulative snow volume to highlight potential watershed-scale snowpack sensitivity to warming and shifts from snow to rain. Changes in the importance of aspect with SW:NetR↓ suggest that decreases in SW:NetR↓ caused by regional warming, changes in humidity or cloud cover, as well as shifts to earlier peak SWE, will likely produce differential effects on mountain snowpacks. This study demonstrates the utility of airborne lidar surveys for evaluating how physiography and regional climate interact to determine watershed-level snow distributions and helps better inform how climate will affect vital western U.S. snowpack and water resources.

Acknowledgments
During the preparation of this manuscript, C. J. Tennant was supported by NSF RC CZO Cooperative Agreement EAR 1331872, USDA ARS and a NSF CZO SAVI Award 1445246. A Gordon and Betty Moore Foundation Data-Driven Discovery Investigator award provided additional support to L. G. Larsen and C. J. Tennant. Lidar data were collected by NCALM under awards EAR-0922307 (Jemez), EPS-0447689 (Reynolds), EAR-0922307 (Sierra). A. A. Harpold was supported by USDA NIFA NEV05293 and NASA Experimental Program to Stimulate Competitive Research (EPSCoR) Cooperative Agreement NNX14AN24A. Additional support was provided by NSF EPSCoR award OIA-1208732 and NSF EAR-1331408. The climate metrics used in this study were downloaded from NASA's Giovanni data portal (http://giovanni.gsfc.nasa.gov/giovanni/) and the snow depth, terrain, and canopy-height models for BCW, JRB, KREW, and WOLV were obtained from http://www.opentopography.org/. KREW is labeled Providence Creek on OpenTopography. The snow depth, terrain, and canopy-height models for RCEW were obtained from Nancy Glenn and are available at http://scholarworks.boisestate.edu/bcal_data/4/. We thank Adam Winstral for a careful review that allowed us to correct errors in an initial data set and for his thoughtful comments which greatly improved the study. We also thank associate editor Charlie Luce and two anonymous reviewers for insightful comments that significantly increased the quality of the manuscript.

References

Adams, W. (1976), Areal differentiation of snow cover in east central Ontario, *Water Resour. Res.*, *12*(6), 1226–1234.
Agresti, A. (1996), *An Introduction to Categorical Data Analysis*, Wiley, New York.
Anderson, B. T., J. P. McNamara, H. P. Marshall, and A. N. Flores (2014), Insights into the physical processes controlling correlations between snow distribution and terrain properties, *Water Resour. Res.*, *50*, 4545–4563, doi:10.1002/2013WR013714.
Anderson, S. P., G. Qinghua, and E. G. Parrish (2012), *Snow-on and Snow-off Lidar Point Cloud Data and Digital Elevation Models for Study of Topography, Snow, Ecosystems and Environmental Change at Southern Sierra Critical Zone Observatory* [digital media], Univ. of California at Merced, Southern Sierra CZO, Calif.
Bales, R. C., J. W. Hopmans, A. T. O'Geen, M. Meadows, P. C. Hartsough, P. Kirchner, C. T. Hunsaker, and D. Beaudette (2011), Soil moisture response to snowmelt and rainfall in a Sierra Nevada mixed-conifer forest, *Vadose Zone J.*, *10*(3), 786–799.
Balk, B., and K. Elder (2000), Combining binary decision tree and geostatistical methods to estimate snow distribution in a mountain watershed, *Water Resour. Res.*, *36*(1), 13–26.
Barnhart, T. B., N. P. Molotch, B. Livneh, A. A. Harpold, J. F. Knowles, and D. Schneider (2016), Snowmelt rate dictates streamflow, *Geophys. Res. Lett.*, *43*, 8006–8016, doi:10.1002/2016GL069690.
Berghuijs, W. R., R. A. Woods, and M. Hrachowitz (2014), A precipitation shift from snow towards rain leads to a decrease in streamflow, *Nat. Clim. Change*, *4*(7), 583–586.
Biederman, J. A., P. D. Brooks, A. A. Harpold, D. J. Gochis, E. Gutmann, D. E. Reed, E. Pendall, and B. E. Ewers (2014), Multiscale observations of snow accumulation and peak snowpack following widespread, insect-induced lodgepole pine mortality, *Ecohydrology*, *7*(1), 150–162.
Blöschl, G., R. Kirnbauer, and D. Gutknecht (1991a), Distributed snowmelt simulations in an alpine catchment: 1: Model evaluation on the basis of snow cover patterns, *Water Resour. Res.*, *27*(12), 3171–3179.
Blöschl, G., D. Gutknecht, and R. Kirnbauer (1991b), Distributed snowmelt simulations in an alpine catchment: 2: Parameter study and model predictions. *Water Resour. Res.*, *27*(12), 3181–3188.
Brooks, P. D., P. Grogan, P. H. Templer, P. Groffman, M. G. Öquist, and J. Schimel (2011), Carbon and nitrogen cycling in snow covered environments, *Geogr. Compass*, *5*(9), 682–699.
Broxton, P. D., A. A. Harpold, J. A. Biederman, P. A. Troch, N. P. Molotch, and P. D. Brooks (2015), Quantifying the effects of vegetation structure on snow accumulation and ablation in mixed-conifer forests, *Ecohydrology*, *8*(6), 1073–1094.
Casola, J. H., L. Cuo, B. Livneh, D. P. Lettenmaier, M. T. Stoelinga, P. W. Mote, and J. M. Wallace (2009), Assessing the impacts of global warming on snowpack in the Washington cascades, *J. Clim.*, *22*(10), 2758–2772.
Chang, K. T., and Z. X. Li (2000), Modelling snow accumulation with a geographic information system, *Int. J. Geogr. Inform. Sci.*, *14*(7), 693–707.
Clark, M. P., J. Hendrikx, A. G. Slater, D. Kavetski, B. Anderson, N. J. Cullen, T. Kerr, E. O. Hreinsson, and R. A. Woods (2011), Representing spatial variability of snow water equivalent in hydrologic and land-surface models: A review, *Water Resour. Res.*, *47*, W07539, doi:10.1029/2011WR010745.
Cline, D., S. Yueh, B. Chapman, B. Stankov, A. Gasiewski, D. Masters, K. Elder, R. Kelly, T. H. Painter, and S. Miller (2009), NASA cold land processes experiment (CLPX 2002/03): Airborne remote sensing, *J. Hydrometeorol.*, *10*(1), 338–346.
Deems, J. S., T. H. Painter, and D. C. Finnegan (2013), Lidar measurement of snow depth: A review, *J. Glaciol.*, *59*(215), 467–479.
Dettinger, M., K. Redmond, and D. Cayan (2004), Winter orographic precipitation ratios in the Sierra Nevada-Large-scale atmospheric circulations and hydrologic consequences, *J. Hydrometeorol.*, *5*(6), 1102–1116.
Elder, K., J. Dozier, and J. Michaelsen (1991), Snow accumulation and distribution in an alpine watershed, *Water Resour. Res.*, *27*(7), 1541–1552.
Elsen, P. R., and M. W. Tingley (2015), Global mountain topography and the fate of Montane species under climate change, *Nat. Clim. Change*, *5*(8), 772–776.
Erickson, T. A., M. W. Williams, and A. Winstral (2005), Persistence of topographic controls on the spatial distribution of snow in rugged mountain terrain, Colorado, United States, *Water Resour. Res.*, *41*, W04014, doi:10.1029/2003WR002973.
Essery, R., N. Rutter, J. Pomeroy, R. Baxter, M. Stähli, D. Gustafsson, A. Barr, P. Bartlett, and K. Elder (2009), SNOWMIP2: An evaluation of forest snow process simulations, *Bull. Am. Meteorol. Soc.*, *90*(8), 1120–1135.
Freedman, D., and P. Diaconis (1981), On the histogram as a density estimator: L 2 theory, *Probab. Theory Related Fields*, *57*(4), 453–476.
Gelfan, A. N., J. W. Pomeroy, and L. S. Kuchment (2004), Modeling forest cover influences on snow accumulation, sublimation, and melt, *J. Hydrometeorol.*, *5*(5), 785–803.
Girotto, M., G. Cortes, S. A. Margulis, and M. Durand (2014), Examining spatial and temporal variability in snow water equivalent using a 27 year reanalysis: Kern River watershed, Sierra Nevada, *Water Resour. Res.*, *50*, 6713–6734, doi:10.1002/2014WR015346.
Godsey, S., J. Kirchner, and C. Tague (2013), Effects of changes in winter snowpacks on summer low flows: Case studies in the Sierra Nevada, California, USA, *Hydrol. Processes*, *28*, 5048–5064.
Goulden, M. L., and R. C. Bales (2014), Mountain runoff vulnerability to increased evapotranspiration with vegetation expansion, *Proc. Natl. Acad. Sci. U. S. A.*, *111*(39), 14,071–14,075.
Gromping, U. (2006), Relative importance for linear regression in R: The package relaimpo, *J. Stat. Software*, *17*(1), 1–27.
Grünewald, T., J. Stotter, J. W. Pomeroy, R. Dadic, I. M. Banos, J. Marturia, M. Spross, C. Hopkinson, P. Burlando, and M. Lehning (2013), Statistical modelling of the snow depth distribution in open alpine terrain, *Hydrol. Earth Syst. Sci.*, *17*(8), 3005–3021.
Grünewald, T., Y. Buhler, and M. Lehning (2014), Elevation dependency of mountain snow depth, *Cryosphere*, *8*(6), 2381–2394.
Guo, Q., and R. Bales, (2012), *Snow-on and Snow-off Lidar Point Cloud Data and Digital Elevation Models for Study of Topography, Snow, Ecosystems and Environmental Change at Southern Sierra Critical Zone Observatory* [digital media], Univ. of California at Merced, Southern Sierra CZO, Calif.
Hanson, C. L. (2001), Long-term precipitation database, Reynolds Creek Experimental Watershed, Idaho, United States, *Water Resour. Res.*, *37*(11), 2831–2834.
Harpold, A. A., et al., (2014a), Lidar-derived snowpack data sets from mixed conifer forests across the Western United States, *Water Resour. Res.*, *50*, 2749–2755, doi:10.1002/2013WR013935.
Harpold, A. A., J. A. Biederman, K. Condon, M. Merino, Y. Korgaonkar, T. Nan, L. L. Sloat, M. Ross, and P. D. Brooks (2014b), Changes in snow accumulation and ablation following the Las Conchas Forest Fire, New Mexico, USA, *Ecohydrology*, *7*(2), 440–452, doi:10.1002/eco.1363.
Harpold, A. A., N. P. Molotch, K. N. Musselman, R. C. Bales, P. B. Kirchner, M. Litvak, and P. D. Brooks (2014c), Soil moisture response to snowmelt timing in mixed-conifer subalpine forests, *Hydrol. Processes*, *29*, 2782–2798, doi:10.1002/hyp.10400.
Hay, L. E., and G. J. McCabe (1998), Verification of the rhea-orographic-precipitation model, *J. Am. Water Resour. Assoc.*, *34*(1), 103–112.
Hedrick, A., H. P. Marshall, A. Winstral, K. Elder, S. Yueh, and D. Cline (2015), Independent evaluation of the SNODAS snow depth product using regional-scale lidar-derived measurements, *Cryosphere*, *9*(1), 13–23.

Hiemstra, C. A., G. E. Liston, and W. A. Reiners (2002), Snow redistribution by wind and interactions with vegetation at upper treeline in the Medicine Bow Mountains, Wyoming, USA, *Arct. Antarct. Alp. Res.*, *34*(3), 262–273.
Hood, E., M. Williams, and D. Cline (1999), Sublimation from a seasonal snowpack at a continental, mid-latitude alpine site, *Hydrol. Processes*, *13*(1213), 1781–1797.
Hopkinson, C., M. Sitar, L. Chasmer, and P. Treitz (2004), Mapping snowpack depth beneath forest canopies using airborne lidar, *Photogr. Eng. Remote Sens.*, *70*(3), 323–330.
Houze, R. A., Jr. (2012), Orographic effects on precipitating clouds, *Rev. Geophys.*, *50*, RG1001, doi:10.1029/2011RG000365.
Hubbart, J. A., T. E. Link, and J. A. Gravelle (2015), Forest canopy reduction and snowpack dynamics in a northern Idaho watershed of the continental-maritime region, United States, *For. Sci.*, *61*(5), 882–894.
Jost, G., M. Weiler, D. R. Gluns, and Y. Alila (2007), The influence of forest and topography on snow accumulation and melt at the watershed-scale, *J. Hydrol.*, *347*(1–2), 101–115.
Kienzle, S. (2004), The effect of DEM raster resolution on first order, second order and compound terrain derivatives, *Trans. GIS*, *8*(1), 83–111.
Kirchner, P. B., R. C. Bales, N. P. Molotch, J. Flanagan, and Q. Guo (2014), lidar measurement of seasonal snow accumulation along an elevation gradient in the southern Sierra Nevada, California, *Hydrol. Earth Syst. Sci.*, *18*(10), 4261–4275.
Klos, P. Z., T. E. Link, and J. T. Abatzoglou (2014), Extent of the rain-snow transition zone in the western U.S. under historic and projected climate, *Geophys. Res. Lett.*, *41*, 4560–4568, doi:10.1002/2014GL060500.
Knowles, J. F., A. A. Harpold, R. Cowie, M. Zeliff, H. R. Barnard, S. P. Burns, P. D. Blanken, J. F. Morse, and M. W. Williams (2015), The relative contributions of alpine and subalpine ecosystems to the water balance of a mountainous, headwater catchment, *Hydrol. Processes*, *29*(22), 4794–4808.
Lopez-Moreno, J. I., and D. Nogues-Bravo (2006), Interpolating local snow depth data: An evaluation of methods, *Hydrol. Processes*, *20*(10), 2217–2232.
Luce, C. H., D. G. Tarboton, and R. R. Cooley (1998), The influence of the spatial distribution of snow on basin-averaged snowmelt, *Hydrol. Processes*, *12*(10–11), 1671–1683.
Luce, C. H., J. T. Abatzoglou, and Z. A. Holden (2013), The missing mountain water: Slower Westerlies decrease orographic enhancement in the Pacific Northwest USA, *Science*, *342*(6164), 1360–1364.
Luce, C. H., V. Lopez-Burgos, and Z. Holden (2014), Sensitivity of snowpack storage to precipitation and temperature using spatial and temporal analog models, *Water Resour. Res.*, *50*, 9447–9462, doi:10.1002/2013WR014844.
Lundquist, J. D., P. J. Neiman, B. Martner, A. B. White, D. J. Gottas, and F. M. Ralph (2008), Rain versus snow in the Sierra Nevada, California: Comparing Doppler profiling radar and surface observations of melting level, *J. Hydrometeorol.*, *9*(2), 194–211.
Lundquist, J. D., J. R. Minder, P. J. Neiman, and E. Sukovich (2010), Relationships between barrier jet heights, orographic precipitation gradients, and streamflow in the northern Sierra Nevada, *J. Hydrometeorol.*, *11*(5), 1141–1156.
Lundquist, J. D., S. E. Dickerson-Lange, J. A. Lutz, and N. C. Cristea (2013), Lower forest density enhances snow retention in regions with warmer winters: A global framework developed from plot-scale observations and modeling, *Water Resour. Res.*, *49*, 6356–6370, doi:10.1002/wrcr.20504.
MacDonald, M., J. Pomeroy, and A. Pietroniro (2010), On the importance of sublimation to an alpine snow mass balance in the Canadian Rocky Mountains, *Hydrol. Earth Syst. Sci.*, *14*(7), 1401–1415.
Marks, D., and J. Dozier (1992), Climate and energy exchange at the snow surface in the alpine region of the Sierra Nevada. 2: Snow cover energy balance, *Water Resour. Res.*, *28*(11), 3043–3054.
Marks, D., K. R. Cooley, D. C. Robertson, and A. Winstral (2001), Long-term snow database, Reynolds Creek Experimental Watershed, Idaho, United States, *Water Resour. Res.*, *37*(11), 2835–2838.
Marks, D., A. Winstral, and M. Seyfried (2002), Simulation of terrain and forest shelter effects on patterns of snow deposition, snowmelt and runoff over a semi-arid mountain catchment, *Hydrol. Processes*, *16*(18), 3605–3626.
Marks, D., A. Winstral, M. Reba, J. Pomeroy, and M. Kumar (2013), An evaluation of methods for determining during-storm precipitation phase and the rain/snow transition elevation at the surface in a mountain basin, *Adv. Water Resour.*, *55*, 98–110.
McVicar, T. R., et al. (2012), Global review and synthesis of trends in observed terrestrial near-surface wind speeds: Implications for evaporation, *J. Hydrol.*, *416*, 182–205.
Minder, J. R. (2010), The sensitivity of mountain snowpack accumulation to climate warming, *J. Clim.*, *23*(10), 2634–2650.
Monson, R. K., A. A. Turnipseed, J. P. Sparks, P. C. Harley, L. E. Scott-Denton, K. Sparks, and T. E. Huxman (2002), Carbon sequestration in a high-elevation, subalpine forest, *Global Change Biol.*, *8*(5), 459–478.
Musselman, K., N. Molotch, and P. Brooks (2008), Effects of vegetation on snow accumulation and ablation in a mid-latitude sub-alpine forest, *Hydrol. Processes*, *22*(15), 2767–2776.
Musselman, K. N., M. P. Clark, C. Liu, K. Ikeda, and R. Rasmussen (2017), Slower snowmelt in a warmer world, *Nat. Clim. Change*, *7*(3), 214–219.
Painter, T. H., et al. (2016), The Airborne Snow Observatory: Fusion of scanning lidar, imaging spectrometer, and physically-based modeling for mapping snow water equivalent and snow albedo, *Remote Sens. Environ.*, *184*, 139–152.
Pepin, N., et al. (2015), Elevation-dependent warming in mountain regions of the world, *Nat. Clim. Change*, *5*, 424–430.
Pomeroy, J. W., and K. Dion (1996), Winter radiation extinction and reflection in a boreal pine canopy: Measurements and modelling, *Hydrol. Processes*, *10*(12), 1591–1608.
Prasad, R., D. G. Tarboton, G. E. Liston, C. H. Luce, and M. S. Seyfried (2001), Testing a blowing snow model against distributed snow measurements at upper sheep creek, *Water Resour. Res.*, *37*(5), 1341–1356.
R Core Team (2013), R: A language and environment for statistical computing, R Found. for Stat. Comput., Vienna. [Available at http://www.R-project.org/.]
Rhea, J. O. (1977), Orographic precipitation model for hydrometeorological use, *Atmos. Sci. Pap.*, 287.
Rinehart, A. J., E. R. Vivoni, and P. D. Brooks (2008), Effects of vegetation, albedo, and solar radiation sheltering on the distribution of snow in the Valles Caldera, New Mexico, *Ecohydrology*, *1*(3), 253–270.
Roe, G. H. (2005), Orographic precipitation, *Annu. Rev. Earth Planet. Sci.*, *33*, 645–671.
Rutter, N., et al. (2009), Evaluation of forest snow processes models (SnowMIP2), *J. Geophys. Res.*, *114*, D06111, doi:10.1029/2008JD011063.
Ryberg, K. R., F. A. Akyüz, G. J. Wiche, and W. Lin (2015), Changes in seasonality and timing of peak streamflow in snow and semi-arid climates of the north-central United States, 1910–2012, *Hydrol. Processes*, *30*, 1208–1218, doi:10.1002/hyp.10693.
Salzer, M. W., M. K. Hughes, A. G. Bunn, and K. F. Kipfmueller (2009), Recent unprecedented tree-ring growth in bristlecone pine at the highest elevations and possible causes, *Proc. Natl. Acad. Sci. U. S. A.*, *106*(48), 20,348–20,353.
Seager, R., M. F. Ting, C. H. Li, N. Naik, B. Cook, J. Nakamura, and H. B. Liu (2013), Projections of declining surface-water availability for the southwestern United States, *Nat. Clim. Change*, *3*(5), 482–486.

Shrestha, R. (2016), 2009 1m Snow Depth for Reynolds Mountain East, Reynolds Creek Experimental Watershed, Idaho [data set], doi: 10.18122/B28597. [Available at http://scholarworks.boisestate.edu/bcal_data/4/.]
Slaughter, C. W., D. Marks, G. N. Flerchinger, S. S. Van Vactor, and M. Burgess (2001), Thirty-five years of research data collection at the Reynolds Creek Experimental Watershed, Idaho, United States, *Water Resour. Res.*, *37*(11), 2819–2823.
Steppuhn, H., and G. Dyck (1974), Estimating true basin snowcover, paper presented at Advanced Concepts and Techniques in the Study of Snow and Ice Resources: An Interdisciplinary Symposium [papers], Natl. Acad., Washington, D. C.
Stewart, I. T., D. R. Cayan, and M. D. Dettinger (2005), Changes toward earlier streamflow timing across western North America, *J. Clim.*, *18*(8), 1136–1155.
Stielstra, C. M., K. A. Lohse, J. Chorover, J. C. McIntosh, G. A. Barron-Gafford, J. N. Perdrial, M. Litvak, H. R. Barnard, and P. D. Brooks (2015), Climatic and landscape influences on soil moisture are primary determinants of soil carbon fluxes in seasonally snow-covered forest ecosystems, *Biogeochemistry*, *123*(3), 447–465.
Sturm, M., B. Taras, G. E. Liston, C. Derksen, T. Jonas, and J. Lea (2010), Estimating snow water equivalent using snow depth data and climate classes, *J. Hydrometeorol.*, *11*(6), 1380–1394.
Tarboton, D., G. Blöschl, K. Cooley, R. Kirnbauer, and C. Luce (2001), Spatial snow cover processes at Kühtai and Reynolds Creek, in *Spatial Patterns in Catchment Hydrology: Observations and Modelling*, edited by R. Grayson and G. Blöschl, pp. 158–186, Cambridge Univ. Press, Cambridge, U. K.
Tennant, C. J., B. T. Crosby, S. E. Godsey, R. W. VanKirk, and D. R. Derryberry (2015a), A simple framework for assessing the sensitivity of mountain watersheds to warming-driven snowpack loss, *Geophys. Res. Lett.*, *42*, 2814–2822, doi:10.1002/2015GL063413.
Tennant, C. J., B. T. Crosby, and S. E. Godsey (2015b), Elevation-dependent responses of streamflow to climate warming, *Hydrol. Processes*, *29*(6), 991–1001.
Tinkham, W. T., A. M. S. Smith, H. P. Marshall, T. E. Link, M. J. Falkowski, and A. H. Winstral (2014), Quantifying spatial distribution of snow depth errors from lidar using Random Forest, *Remote Sens. Environ.*, *141*, 105–115.
Trujillo, E., N. P. Molotch, M. L. Goulden, A. E. Kelly, and R. C. Bales (2012), Elevation-dependent influence of snow accumulation on forest greening, *Nat. Geosci.*, *5*(10), 705–709.
U.S. Army Corps of Engineers (1956), *Snow Hydrology: Summary Report of the Snow Investigations of the North Pacific Division*, Gov. Print. Off., Washington, D. C.
Varhola, A., N. C. Coops, M. Weiler, and R. D. Moore (2010), Forest canopy effects on snow accumulation and ablation: An integrative review of empirical results, *J. Hydrol.*, *392*(3), 219–233.
Veatch, W., P. D. Brooks, J. R. Gustafson, and N. P. Molotch (2009), Quantifying the effects of forest canopy cover on net snow accumulation at a continental, mid-latitude site, *Ecohydrology*, *2*(2), 115–128.
Walters, R. D., K. A. Watson, H. P. Marshall, J. P. McNamara, and A. N. Flores (2014), A physiographic approach to downscaling fractional snow cover data in mountainous regions, *Remote Sens. Environ.*, *152*, 413–425.
Wang, R., M. Kumar, and T. E. Link (2016), Potential trends in snowmelt-generated peak streamflows in a warming climate, *Geophys. Res. Lett.*, *43*, 5052–5059, doi:10.1002/2016GL068935.
Wayand, N. E., J. D. Lundquist, and M. P. Clark (2015), Modeling the influence of hypsometry, vegetation, and storm energy on snowmelt contributions to basins during rain-on-snow floods, *Water Resour. Res.*, *51*, 8551–8569, doi:10.1002/2014WR016576.
Wetlaufer, K., J. Hendrikx, and L. Marshall (2016), Spatial heterogeneity of snow density and its influence on snow water equivalence estimates in a large mountainous basin, *Hydrology*, *3*(1), 3, doi:10.3390/hydrology3010003.
Winstral, A., and D. Marks (2002), Simulating wind fields and snow redistribution using terrain-based parameters to model snow accumulation and melt over a semi-arid mountain catchment, *Hydrol. Processes*, *16*(18), 3585–3603.
Winstral, A., D. Marks, and R. Gurney (2013), Simulating wind-affected snow accumulations at catchment to basin scales, *Adv. Water Resour.*, *55*, 64–79.
Xia, Y. L., et al. (2012), Continental-scale water and energy flux analysis and validation for the North American Land Data Assimilation System project phase 2 (NLDAS-2). 1: Intercomparison and application of model products, *J. Geophys. Res.*, *117*, D03109, doi:10.1029/2011JD016048.
Zheng, Z., P. B. Kirchner, and R. C. Bales (2016), Topographic and vegetation effects on snow accumulation in the southern Sierra Nevada: A statistical summary from lidar data, edited, *Cryosphere*, *10*, 257–269.